Technical note

Nuclear Medicine Communications

Activity concentration measurements using a conjugate gradient (Siemens xSPECT) reconstruction algorithm in SPECT/CT

Ian S. Armstrong[a] and Sandra A. Hoffmann[b]

The interest in quantitative single photon emission computer tomography (SPECT) shows potential in a number of clinical applications and now several vendors are providing software and hardware solutions to allow 'SUV-SPECT' to mirror metrics used in PET imaging. This brief technical report assesses the accuracy of activity concentration measurements using a new algorithm 'xSPECT' from Siemens Healthcare. SPECT/CT data were acquired from a uniform cylinder with 5, 10, 15 and 20 s/projection and NEMA image quality phantom with 25 s/projection. The NEMA phantom had hot spheres filled with an 8 : 1 activity concentration relative to the background compartment. Reconstructions were performed using parameters defined by manufacturer presets available with the algorithm. The accuracy of activity concentration measurements was assessed. A dose calibrator–camera cross-calibration factor (CCF) was derived from the uniform phantom data. In uniform phantom images, a positive bias was observed, ranging from ~6% in the lower count images to ~4% in the higher-count images. On the basis of the higher-count data, a CCF of 0.96 was derived. As expected, considerable negative bias was measured in the NEMA spheres using region mean values whereas positive bias was measured in the four largest NEMA spheres. Nonmonotonically increasing recovery curves for the hot spheres suggested the presence of Gibbs edge enhancement from resolution modelling. Sufficiently accurate activity concentration measurements can easily be measured on images reconstructed with the xSPECT algorithm without a CCF. However, the use of a CCF is likely to improve accuracy further. A manual conversion of voxel values into SUV should be possible, provided that the patient weight, injected activity and time between injection and imaging are all known accurately. *Nucl Med Commun* **37:1212–1217**

Nuclear Medicine Communications 2016, **37**:1212–1217

Keywords: quantification, reconstruction, SPECT

[a]Department of Nuclear Medicine, Central Manchester University Hospitals, Manchester and [b]Department of Nuclear Medicine, Salford Royal NHS Foundation, Salford, UK

Correspondence to Ian S. Armstrong, MPhys, MSc, Nuclear Medicine Centre, Central Manchester University Hospitals, NHS Foundation Trust, Oxford Road, Manchester M13 9WL, UK
Tel: +44 161 276 4785; fax: +44 161 276 8023;
e-mail: ian.armstrong@cmft.nhs.uk

Received 25 May 2016 **Revised** 28 June 2016 **Accepted** 20 July 2016

Introduction

Hybrid gamma cameras offering combined multiple-detector single photon emission computer tomography (SPECT) acquisition combined with computed tomography (CT) have been available for ~15 years. With advances in image reconstruction technology and more comprehensive data corrections (CT-attenuation, scatter and resolution modelling), SPECT images have the potential to provide fully quantitative uptake measures to mirror the images produced from PET systems. The interest in quantitative SPECT is beginning to gather momentum with a number of potential clinical applications [1–4]. Unlike PET, units of the voxel data in SPECT have traditionally been counts instead of explicitly Bq/ml. Consequently, voxel values increase with increasing SPECT scan time and hence an acquisition-dependent calibration factor is required. Recently, a new variant of the iterative reconstruction algorithm has become available from Siemens Healthcare on new Symbia Intevo gamma cameras. Siemens 'xSPECT' uses an ordered subset conjugate gradient maximization (OSCGM) algorithm to produce reconstructed SPECT images [5]. Perhaps most importantly in terms of quantification, voxel values have units of Bq/ml and are hence independent of imaging time of the SPECT scan. Given that there is no explicit cross-calibration factor (CCF) between the ionization dose calibrator and the gamma camera, the accuracy of such measurements is not guaranteed. This brief technical paper aims to assess the accuracy of activity concentration measurements using xSPECT reconstruction in phantom acquisitions.

Methods

Uniform phantom

A 20 cm diameter uniform cylindrical phantom with a volume of 6280 ml was filled with 150 MBq of Tc-99m to yield an activity concentration of 23.9 kBq/ml. The phantom was agitated and left for 30 min to ensure adequate mixing of the radioactivity.

The phantom was positioned at the centre of the field of view of a Siemens Symbia Intevo T2 (Siemens Medical

0143-3636 DOI: 10.1097/MNM.0000000000000586

Solutions, Erlangen, Germany) using the CT lasers. Four SPECT/CT acquisitions were acquired with a 360° orbit, autocontouring, a matrix of 256 × 256, zoom of 1.0 (pixel size 2.4 mm), photopeak energy window of 129–150 keV and scatter energy window of 108–129 keV. The time per projection was adjusted for each SPECT acquisition and set as 20, 15, 10 and 5 s. A CT scan for attenuation correction was performed with 130 kV, CAREdose (Siemens Medical Solutions, Erlangen, Germany) dose modulation with a quality reference of 60 mAs, a slice thickness of 3.0 mm and a pitch of 2.0.

Images were reconstructed with the OSCGM algorithm using five available presets for iterations (i) and subsets (s). These were 24i2s, 48i1s, 60i1s, 72i1s and 84i1s. Data were reconstructed without any postfiltering and also a 5.0 mm full-width-half-maximum (FWHM) Gaussian filter. Attenuation correction using the CT image was performed. Scatter correction was performed using a dual-energy window method. The scatter images were smoothed with a 12 mm FWHM Gaussian filter before incorporating into the reconstruction, which is the standard procedure applied by the manufacturer.

NEMA image quality phantom

The background section of a NEMA image quality phantom (PTW, Breisgau, Germany) was filled with Tc-99m to an activity concentration of 19.4 kBq/ml and all six spheres (10, 13, 17, 22, 28 and 37 mm diameter) with an activity concentration of 158 kBq/ml. A single SPECT/CT was performed using the same parameters for the uniform phantom, with the exception of the time per projection, which was set at 25 s. OSCGM reconstructions using the same five presets without postfiltering were performed along with two additional reconstructions using 48i1s with a 5 mm FWHM Gaussian postfilter and a 10 mm FWHM Gaussian postfilter.

Image analysis

All image data were analysed off-line in Matlab (The MathsWorks, Natick, Massachusetts, USA) to ensure vendor neutrality with voxel values read from the data as Bq/ml. For the uniform phantom data, a cylindrical region, 14 cm in diameter and 12 cm in length, was placed at the centre of the phantom. The mean and SD of voxel values within the region were obtained from each image. For the NEMA data, spherical regions with diameters equalling the physical spheres were placed over each sphere. The region mean and region maximum voxel values were measured from each sphere and each image. Twelve regions were drawn in the background compartment and the mean and SD of voxels within each region was calculated. All activity concentration measurements were compared with the known values after accounting for decay of the Tc-99m from the measurement time to the starting time of each SPECT acquisition. For the uniform phantom and NEMA background, the percentage bias of mean activity concentration was calculated. For the NEMA spheres, the recovery coefficient (ratio of measured/known) was calculated for both the region mean and the region maximum voxel values. For each NEMA sphere, the signal to noise ratio (SNR) was also calculated as

$$\mathrm{SNR} = \frac{(A_S - A_{BG})}{\sigma_{BG}},$$

where, A_S and A_{BG} are the activity concentrations measured in the spheres and background, respectively, and σ_{BG} is the voxel SD in the background.

Results

Uniform cylinder

Figure 1 shows the percentage bias of the measured activity concentrations for each of the four SPECT acquisitions and also the voxel noise (expressed as coefficient of variation) in the uniform phantom for each SPECT acquisition. The data show that the bias reduces with increasing projection time. This is expected because of a reduction in the contribution of noise, which is shown to decrease with increasing projection time as expected and the low-count bias that is associated with expectation maximization algorithms [6]. The reconstruction with the lowest voxel noise was 48 iterations and one subset in the 20 s/projection image. Figure 1a and c shows that there is negligible difference in the activity concentration measurements as iterations increase from 48 to 84 in the reconstructions with one subset. A CCF of 0.96 was derived from the 48i1s 20 s/projection image with the rationale that this was the least noisy image.

NEMA image quality

The activity concentration recovery for unsmoothed and smoothed data using the region mean and region maximum are shown in Fig. 2. A negative bias is observed for all sphere sizes in the region mean measurements, with negative bias worsening in the smaller spheres because of partial volume effects. The differences observed in the region mean recovery for the various reconstructions parameters are negligible. The shape of the recovery curve does not increase monotonically. On the basis of similar data from studies in PET [7], we believe that this is because of constructive interference of Gibbs edge enhancement artefacts at particular sphere sizes arising from the resolution modelling in the reconstruction [8].

A positive bias is observed for the four largest spheres without the use of postfiltering for the region maximum recovery values. The choice of reconstructions parameters has a greater impact on the recovery. The application of postfiltering has a more marked impact on the activity concentration measurements using the maximum

Fig. 1

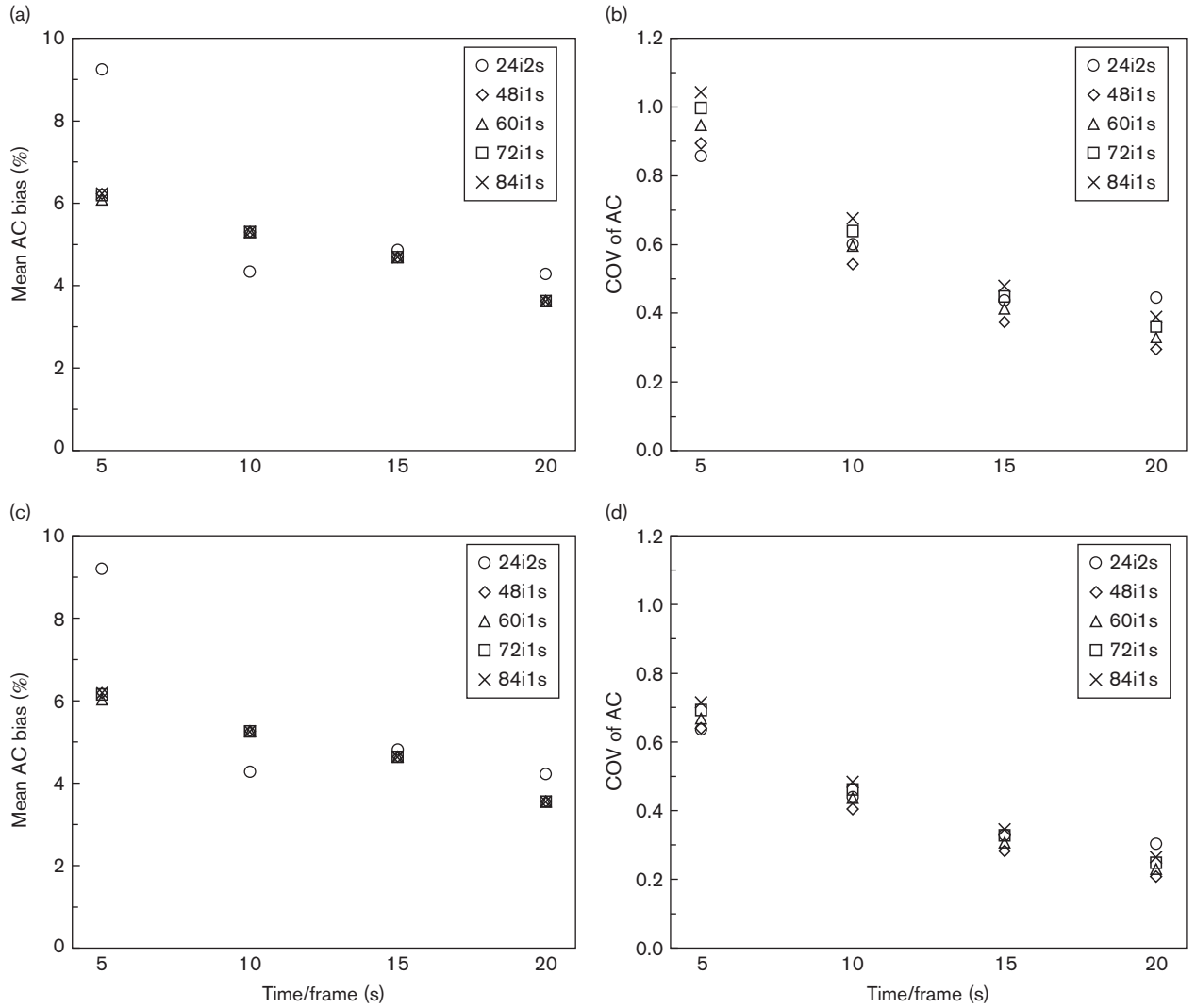

(a, c) Percentage bias of the activity concentration measurements in the uniform phantom against time per projection. (b, d) Coefficient of variation (COV) of voxel values in the region of interest in the uniform phantom against time per projection. Data are shown without postfiltering (a, b) and with 5 mm Gaussian postfiltering (c, d). AC, activity concentration; 24i2s, 24 iterations and two subsets; 48i1s, 48 iterations and one subset; 60i1s, 60 iterations and one subset; 72i1s, 72 iterations and one subset; 84i1s, 84 iterations and one subset.

voxel. These two observations are likely to be the greater contribution of image noise to the measurements.

Measurements of the NEMA background activity concentration without and with the CCF derived from the uniform phantom are shown in Fig. 3. Finally, the SNR results for the hot spheres using region mean and region maximum are shown in Fig. 4.

Discussion

This study has assessed the accuracy of activity concentration measurements from Siemens xSPECT images where no explicit CCF between the dose calibrator and the gamma camera has been defined. In the uniform cylinder SPECT acquisitions, the bias in measurements ranged from ~6% in the lower count images to ~4% in the higher-count images. We consider this to be very good performance considering the lack of CCF applied for this data. Using the CCF derived from the uniform phantom, bias reduced to ~−1% in the NEMA background. The phantom data from which the CCF was derived were still relatively low in the number of counts acquired because of the modest level of activity used and the relatively short scan time. In practice, it may be advantageous to perform a higher-count SPECT scan on a routine monthly basis to assess the stability of a CCF.

It is interesting from Fig. 1 to note that the reconstruction with 24 iterations and two subsets produces a notable discrepancy in measured activity concentration

Fig. 2

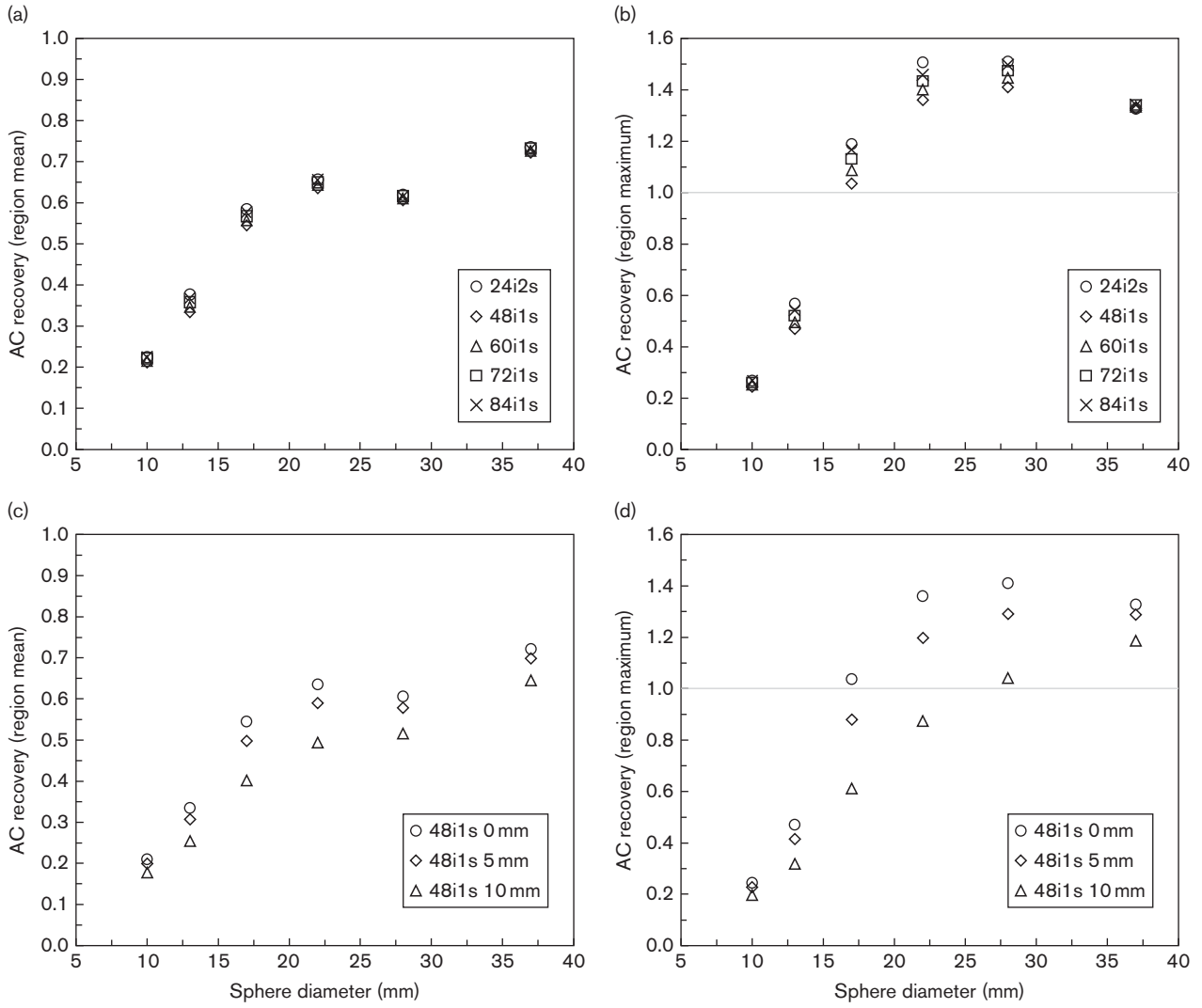

Recovery coefficient of activity concentration for the six hot spheres using the region mean value (a, c) and using the region maximum value (b, d). Data in the top two plots (a, b) are without postfiltering, whereas data in the lower two plots (c, d) are with varying postfiltering. Data are shown without the use of the cross-calibration factor derived from the uniform cylinder. AC, activity concentration; 24i2s, 24 iterations and two subsets; 48i1s, 48 iterations and one subset; 60i1s, 60 iterations and one subset; 72i1s, 72 iterations and one subset; 84i1s, 84 iterations and one subset; 48i1s 0 mm, 48 iterations and one subsets no postfilter; 48i1s 5 mm, 48 iterations and one subsets with 5 mm Gaussian filter; 48i1s 10 mm, 48 iterations and one subset with 10 mm Gaussian filter.

measurements compared with the reconstructions with one subset. It is also interesting to note for these reconstruction parameters that the voxel noise is the greatest in the 20 s/projection uniform phantom and the SNR is the lowest in the NEMA data. As such, it is likely that using reconstructions parameters with one subset is likely to provide superior results. For the one-subset reconstructed images, the number of iterations used in this study has very little impact on quantification for measurements in uniform areas or the region means of the NEMA spheres. The more apparent impact is increasing image noise, which may also explain the greater increases in the NEMA sphere measurements derived from the region maximum. As shown in Fig. 4, the greatest SNR is achieved with 48 iterations. For the given parameter presets, this is the lowest number of iterations for one subset reconstructions. It may therefore be possible to further optimize the reconstruction by reducing the number of iterations with one subset. This is beyond the scope of this brief report, which intends to show the accuracy using the reconstruction parameter presets that are available to the user in this new reconstruction.

The measurements derived from the images in this work had units of raw activity concentration in Bq/ml. In PET, which also has voxel values in the same units, a

Fig. 3

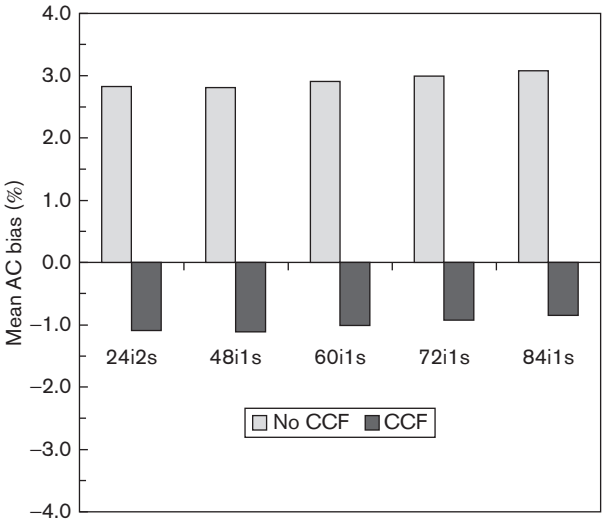

Measurement of activity concentration bias in the background of the NEMA phantom. Data are shown without and with the cross-calibration factor (CCF) applied. AC, activity concentration; 24i2s, 24 iterations and two subsets; 48i1s, 48 iterations and one subset; 60i1s, 60 iterations and one subset; 72i1s, 72 iterations and one subset; 84i1s, 84 iterations and one subset.

conversion into SUV is performed by the display software by normalizing the voxel values to decay-corrected injected activity and patient body weight to provide clinically relevant information. For PET, these factors are part of the DICOM header information and the conversion is automatic. In the case here, an automatic conversion could not be performed because of differences in the DICOM header information. Despite this, we believe that, by echoing the careful practice that is already performed in PET, it should be possible to manually convert the voxel values obtained from the xSPECT into SUV. This will require an accurate measurement of patient weight and the injected activity including a measurement of residual syringe activity following injection. The time between the injection and imaging will need to be known. This manual conversion process may be too arduous for routine use in high-throughput centres, but may be of value when scan numbers are relatively low or perhaps as part of research studies. As with fluorine-18-fluorodeoxyglucose PET imaging, the move to quantitative SPECT is likely to require a tighter control on patient preparation (for example hydration levels in bone scans) and imaging procedures (a well-defined time between injection and imaging) to ensure that measurements are reliable.

Conclusion

The new OSCGM reconstruction algorithm 'xSPECT' from Siemens that is available on Symbia Intevo gamma cameras allows for accurate activity concentration measurements to be derived with ease from reconstructed images. Acceptable results (3–6% bias) were achieved without a CCF. Deriving a CCF from the uniform phantom reduced the bias further to ~1% in magnitude in uniform phantom areas. For clinical applications, a manual conversion of voxel activity concentration measurements into SUV should be possible, provided that

Fig. 4

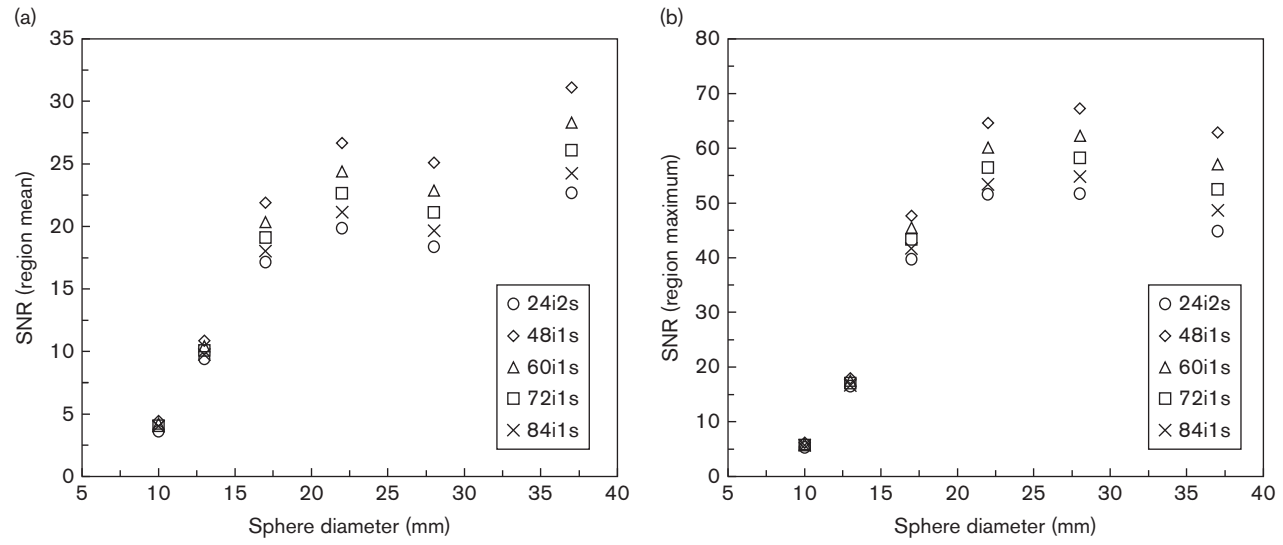

Signal-to-noise ratio (SNR) of the hot spheres in the NEMA phantom for region mean (a) and region maximum (b) measurements. 24i2s, 24 iterations and two subsets; 48i1s, 48 iterations and one subsets; 60i1s, 60 iterations and one subset; 72i1s, 72 iterations and one subset; 84i1s, 84 iterations and one subset.

the patient weight, injected activity and time between injection and imaging are all known accurately.

Acknowledgements

Conflicts of interest

There are no conflicts of interest.

References

1 Kao YH, Tan AEH, Burgmans MC, Irani FG, Khoo LS, Lo RHG, *et al*. Image-guided personalized predictive dosimetry by artery-specific SPECT/CT partition modeling for safe and effective ^{90}Y radioembolization. *J Nucl Med* 2012; **53**:559–566.

2 Garin E, Lenoir L, Rolland Y, Edeline J, Mesbah H, Laffont S, *et al*. Dosimetry based on ^{99m}Tc-macroaggregated albumin SPECT/CT accurately predicts tumor response and survival in hepatocellular carcinoma patients treated with ^{90}Y-loaded glass microspheres: preliminary results. *J Nucl Med* 2012; **53**:255–263.

3 Bailey DL, Willowson KP. An evidence-based review of quantitative SPECT imaging and potential clinical applications. *J Nucl Med* 2013; **54**:83–89.

4 Cachovan M, Vija AH, Hornegger J, Kuwert T. Quantification of ^{99m}Tc-DPD concentration in the lumbar spine with SPECT/CT. *EJNMMI Res* 2013; **3**:45.

5 Vija HA. *Introduction to xSPECT* technology: evolving multi-modal SPECT to become context-based and quantitative Siemens Healthcare White Paper*. Hoffmann Estates, Illinois: Siemens Medical Solutions; 2013.

6 Jian Y, Planeta B, Carson RE. Evaluation of bias and variance in low-count OSEM list mode reconstruction. *Phys Med Biol* 2015; **60**:15–29.

7 Matheoud R, Ferrando O, Valzano S, Lizio D, Sacchetti G, Ciarmiello A, *et al*. Performance comparison of two resolution modeling PET reconstruction algorithms in terms of physical figures of merit used in quantitative imaging. *Phys Med* 2015; **31**:468–475.

8 Rahmim A, Qi J, Sossi V. Resolution modeling in PET imaging: theory, practice, benefits, and pitfalls. *Med Phys* 2013; **40**:064301.